

Lifetime and Coherence of Two-Level Defects in a Josephson Junction

Yoni Shalibo¹, Ya'ara Rofe¹, David Shwa¹, Felix Zeides¹, Matthew Neeley², John M. Martinis² and Nadav Katz¹

¹*Racah Institute of Physics, The Hebrew University of Jerusalem, Jerusalem 91904, Israel and*

²*Department of Physics, University of California, Santa Barbara, California 93106, USA*

We measure the lifetime (T_1) and coherence (T_2) of two-level defect states (TLSs) in the insulating barrier of a Josephson phase qubit and compare to the interaction strength between the two systems. We find for the average decay times a power law dependence on the corresponding interaction strengths, whereas for the average coherence times we find an optimum at intermediate coupling strengths. We explain both the lifetime and the coherence results using the standard TLS model, including dipole radiation by phonons and anti-correlated dependence of the energy parameters on environmental fluctuations.

Two-level defects in amorphous insulators are of fundamental interest due to their impact on many low temperature properties, such as the heat conductivity [1] and the generation of $1/f$ noise [2, 3]. On the practical side, these effects limit the operation of solid state devices, for example amplifiers [4] and CCD detectors [5], and increase the dielectric loss of insulators [6].

Recently, a new type of solid state device has emerged in which quantum coherence is maintained over a large distance. In particular, superconducting Josephson qubits allow one to study quantum coherence at the macroscopic level [7]. Two-level defects in their amorphous oxide tunnel barriers (usually made of AlO_x ($x \approx 1$) [8]) have been found to limit the performance of these devices [6, 9, 10]. In the phase qubit, it was found that at certain biases the qubit is strongly coupled to spurious two-level states (TLSs) which result in free oscillations with the qubit and effectively reduce its coherence [11]. Similar effects have been observed in the flux qubit as well [12], although these are less common due to its smaller junction. Superconducting qubits hold promising features for the implementation of quantum information processing devices, however a significant improvement in defect density is required for future progress.

These defects are thought to arise from charge fluctuators in the insulating material of the junction, presumably O-H bonds [6]. Measurements on dielectrics at high temperature and power combined with measurements on the phase qubit at low temperature strongly support a two-level model for these fluctuators, emerging from tunneling between two configurational states of the charge inside the junction. The notion of coupling of the phase qubit to a strongly anharmonic microscopic system was further fortified through careful analysis of the multilevel spectrum of the phase qubit near resonance with a defect [13]. Neeley *et al.* have demonstrated coherent control over a single defect, and characterized its coherence and relaxation time [14]. Other attempts are being made to reduce the impact of defects by improving junction materials using epitaxial growth [15] or by fabricating dielectric free junctions [16].

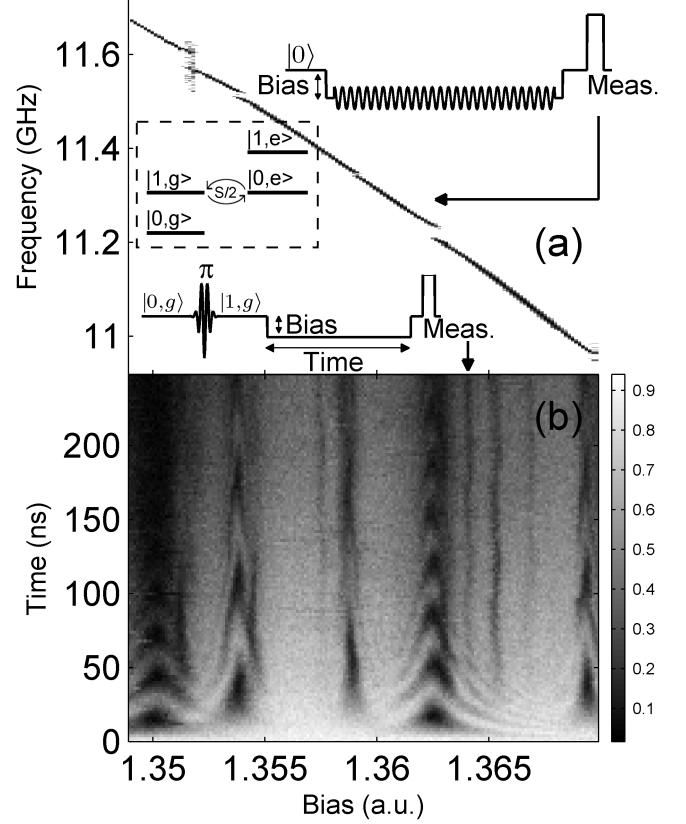


Figure 1: Frequency-domain and time-domain signatures of TLSs in qubit measurement. (a) The probability of the qubit being excited (P_1 , normalized) after a long microwave tone at different frequencies and biases. On top of the expected smooth change of qubit frequency with bias, we observe randomly scattered splittings due to coupling to TLSs. (b) P_1 after qubit excitation followed by a “free” evolution at different bias values. P_1 oscillates near resonance with TLSs, consistent with the position of splittings in the spectrum. Upper and lower insets: control sequences used to produce (a) and (b) respectively. $|0,g\rangle$ and $|1,g\rangle$ stand for states where the qubit is at its ground and excited state respectively while the TLS is at its ground state. Dashed inset: level diagram for the combined qubit-TLS system on resonance.

Several mechanisms have been proposed for relaxation and dephasing of the dielectric defects themselves. En-

ergy relaxation is caused by coupling to phonon states, while dephasing could be caused by spectral diffusion [1]. However, to date, only limited measurements were carried out on TLSs to characterize these processes at the single defect level [17]. Such measurements could be used to better understand the nature of the defects and their decay mechanisms, and possibly engineer long-lived quantum memories in future devices. In [17], the coherence times of several TLSs were measured spectroscopically and were found to distribute as $P \sim 1/T_2$, where T_2 is the spectroscopic coherence time. Neeley's method [14] of probing the TLS adds the capability of measuring the coherence time more accurately and also measure their lifetime separately.

In this letter, we present a measurement of the decay of energy and coherence for a large ensemble of TLSs in a small area junction using the phase qubit. We find that on average, the energy relaxation time (T_1), follows a power law dependence on the coupling parameter to the phase qubit. The exponent of this power law is in fair agreement with what is expected from phonon radiation by a dipole (proportional to the coupling strength) inside the junction. The average dephasing time ($T_\phi = (1/T_2 - 1/2T_1)^{-1}$) is coupling dependent as well, peaking at intermediate couplings. We interpret this optimum coupling to be caused by anti-correlated fluctuations in the physical parameters which determine the TLS energy.

For small area junctions ($\sim 1 \mu m^2$), the typical measurement bandwidth allows us to detect and measure about 10 TLSs in a particular cooldown. Instead of using many different samples to acquire sufficient statistics, we use the fact that heating resets the TLS characteristics. The device is thermally anchored to the mixing chamber of a dilution refrigerator during measurement. We find that the TLS distribution is reset upon raising the temperature above 20 K and cooling down to the base temperature (10 mK). Some memory of the TLS distribution remains if the temperature is increased to only 1.5 K [18]. We utilize this feature to produce a new set of TLSs and generate an ensemble. The data was taken over 82 different TLSs, obtained from 8 different cooldowns.

The initial identification of TLSs and their coupling parameters are carried out as follows. First, the qubit spectrum is swept over the bias [22] to locate the frequencies of TLSs from the positions of the avoided level crossing structures (see Fig. 1a). A complementary picture of the interacting qubit-TLS system in the time domain is shown in Fig. 1b, where we excite the qubit with a short resonant pulse (π -pulse) far away from any observable TLS and then apply a bias pulse of varying amplitude and length. As seen in the figure, for bias values where the qubit is resonant with a TLS we observe oscillations that have the same frequency as the splitting size in the spectrum.

Following Neeley *et al.* [14], the characteristic energy

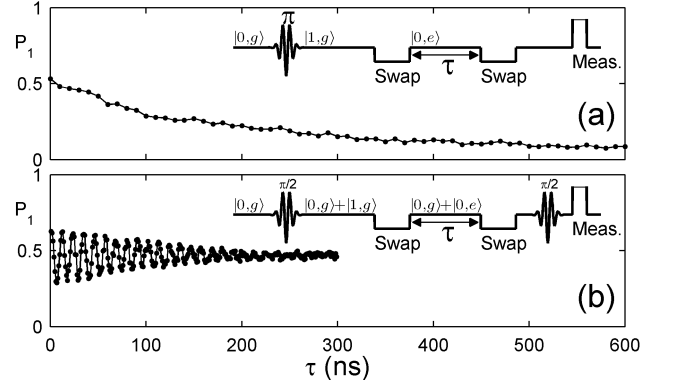


Figure 2: Representative T_1 and T_2 measurements of a TLS. (a) T_1 measurement of the TLS, along with its experimental sequence (inset). The qubit is first excited with a π -pulse, then brought into resonance with a TLS for a “swap time” (the time to fully transfer an excitation between the qubit and the TLS). It is found for each TLS by locating the first minimum in the oscillations in Fig. 1b). After a free evolution of the TLS of time τ , a swap gate is again applied, after which the qubit excitation probability P_1 is measured. (b) T_2 measurement of a TLS, along with its experimental sequence (inset). This sequence is similar to a T_1 measurement, only that superposition states are produced in the TLS and their decay is measured vs. time (Ramsey sequence [14]). The amplitude of the oscillations is proportional to the degree of coherence in the TLS.

relaxation and decoherence time scales were extracted from T_1 and Ramsey experiments on the TLS, with sequences schematically represented in the insets of Fig. 2. Figure 2a and 2b show representative T_1 and T_2 decay curves of the same TLS with characteristic times of 187 ns and 148 ns respectively, obtained from a fit to a decaying exponent and an oscillatory decaying exponent. The size distribution of the observed splittings (see Fig. 3a) follows the theoretical curve predicted by the standard model for two-level defects and agrees with previous results on similar junctions (generated by measuring different samples) [6]. The maximal splitting size is found to be 45 MHz. Theory predicts [6] that this maximal splitting S_{\max} depends on junction parameters and defect size according to $S_{\max} = (2d/x) \sqrt{e^2 E_{10}/2C}$, where x is the barrier thickness, d is the spatial size of the dipole, C is the junction capacitance and E_{10} is the qubit energy. From the measured S_{\max} and known junction parameters we compute a dipole size $d \simeq 1 \text{ \AA}$. The minimal observable splitting size is $\sim 3 \text{ MHz}$, and is mainly limited by the coherence time of the qubit. In addition, we find the distribution of TLS energies (E_{ge} , the energy between the ground state and excited state) to be constant throughout our qubit measurement bandwidth (see Fig. 3b), consistent with theory.

Although most of the T_1 decay curves of the TLSs are similar in their shape (i.e. a simple exponential decay), their decay times range almost 3 orders of magnitude,

from 12 ns to more than 6000 ns. Coherence times on the other hand range from 30 ns to only 150 ns (excluding a single anomalous TLS which will be discussed later). For comparison, when the qubit is biased far from any observable splitting, its lifetime is 270 ns, and its coherence time is 90 ns. TLS energy relaxation times at a given splitting are not random. We find that they are shorter for larger splittings (stronger interaction with the qubit), although short lifetimes are measured for the smallest splittings as well. This trend is apparent in Fig. 3c where we plot average T_1 values as a function of splitting. In this plot we divide the ensemble into groups of TLSs having similar splitting values, in a 7 MHz window size. The error bar represents the statistical spread of the data within this window [18]. We find the average values $\langle T_1(S) \rangle$, excluding two points [18], to be best fitted by a power law $T_1 \propto S^\alpha$, where $\alpha = -1.44 \pm 0.15$ [18]. Figure 3d (black circles) shows the processed T_2 data, obtained similarly from only 43 different TLSs [18]. In this case we observe a weak dependence on the coupling with a peak at $S \approx 25$ MHz. This feature is more pronounced in the dephasing time T_ϕ , represented by red triangles in Fig. 3d.

The T_1 results can be understood within the standard TLS model. The excited state of the TLS involves a local deformation of the insulator. This deformation couples to phonon modes, leading to the decay of the TLS excitation. The expected lifetime for such a process [1], is given by

$$T_1^{-1} = \frac{E_{\text{ge}} \Delta_0^2 \gamma^2}{2\pi \rho \hbar^4} \left(\frac{1}{v_l^5} + \frac{2}{v_t^5} \right), \quad (1)$$

where γ is the deformation potential, v_l and v_t are the speeds of sound for the longitudinal and transverse modes respectively, Δ_0 is the energy splitting due to tunneling and ρ is the mass density. This is consistent with a power law dependence on S , since the interaction strength with the qubit satisfies $S \propto S_{\text{max}} \Delta_0 / E_{\text{ge}}$ [6].

The interaction of a TLS with the qubit is that of an electric dipole with an electric field, and therefore depends on the dipole orientation [6]. This feature explains the large spread in the data at a given splitting: both large dipoles (large Δ_0 / E_{ge}) perpendicular to the junction's electric field and small dipoles aligned with the field can have the same S but different lifetimes. To more rigorously compare experiment with this theory, we simulate an ensemble of TLSs with uniform distribution of dipole orientation and log distribution of dipole moment sizes [6], from which we calculate the average lifetimes as a function of splitting size [18]. The simulation data (see Fig. 3c) yields an average exponent $\alpha = -1.63$ [18], in agreement with our measurement.

The magnitude of the times that we extract from the experiment at a given splitting can be compared to the expected values for defects inside an AlO_x dielectric using

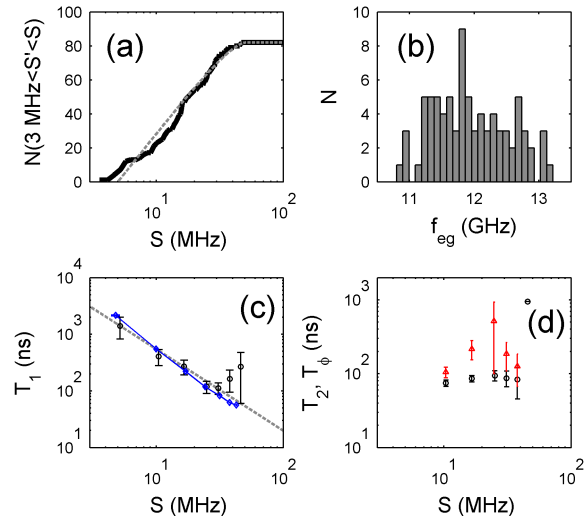


Figure 3: TLS survey results. (a) Frequency and (b) splitting-size distribution of 82 TLSs. The curve in (a) is the best-fitted log-normal distribution of the standard TLS model [6]. (c) Average T_1 values (black circles) as a function of average splittings taken for TLSs inside a 7 MHz splitting window, and the best fitted power law in dashed gray. Average T_1 from stochastic simulation (arbitrary amplitude is shown) in blue diamonds. We attribute the deviation at the largest splittings to low statistics within these windows [18] (d) Average T_2 (black circles) and T_ϕ (red triangles) value as a function of average splitting size within a 7 MHz window.

Eq. 1. We approximate the deformation potential by $\gamma = \frac{1}{2} \rho v^2 \Delta V$ [19], where v is the average speed of sound of the transverse and longitudinal modes and ΔV is the local difference in volumes. For Al_2O_3 values with the difference in volumes taken as $\Delta V \simeq a^3$, where $a \simeq 1$ Å is the extracted dipole size, we get $\gamma \approx 1$ eV, consistent with defects in other dielectrics [3]. Since the dielectric layer thickness is much smaller than the relevant phonon wavelength, the speed of sound in Eq. 1 is set by the aluminum layers of the electrodes. Using the speed of sound for thin aluminum films [20], we get $T_1(S_{\text{max}}) \simeq 30$ ns which is very similar to what we measure. A more specific estimation should take into account the size of the junction and the layered structure.

Assuming the dephasing process is caused by fluctuations in energy, we note that the maximum observed in Fig. 3d can be explained by an anti-correlated dependence of the charging energy and tunneling energy on fluctuations in the TLS environment. According to the TLS model, $E_{\text{ge}} = \sqrt{\Delta^2 + \Delta_0^2}$ where Δ is the energy difference between the bare states of two spatial configurations $|L\rangle$ and $|R\rangle$ and Δ_0 is the tunneling interaction energy. Both Δ and Δ_0 are dependent on a set of environmental parameters \vec{P} , which fluctuate in time. As is standard for the TLS model, we assume a linear sensitivity for Δ on \vec{P} and an exponential sensitivity

for Δ_0 : $\Delta_0(\vec{P}) = N_1 e^{-\sum P_i/P_{0i}}$, $\Delta(\vec{P}) = N_2 \sum P_i/P_{1i}$, with overall dimensional normalization constants N_1 and N_2 and parameter specific constants \vec{P}_0 and \vec{P}_1 . The resulting fluctuations in energy, to first order in fluctuations $\delta\vec{P}$ in these parameters, are given by $\delta E_{\text{ge}} = \frac{1}{E_{\text{ge}}} \sum \delta P_i (\Delta^2/P_{1i} - \Delta_0^2/P_{0i})$. This expansion becomes interesting for the situation where $\Delta_0 \sim \Delta$ as there is a possibility for the contribution in δE_{ge} to pairwise cancel. Since $\Delta_0 = S(E_{\text{ge}}/S_{\text{max}} \cos \eta)$, where η is the dipole orientation relative to the junction's electric field, we expect to find such a cancellation at a particular splitting S . Note that the dependence on $\cos \eta$ smears this somewhat but we still expect a significant effect, as is observed in Fig. 3d.

As seen in the figures, the power-law describing $T_1(S)$ cannot explain all the measured TLSs. We find that three out of 82 TLSs with large splittings (37 MHz, 41 MHz and 45 MHz) have much longer lifetimes than expected (220 ns, 243 ns and 476 ns - respectively). In addition, one TLS out of 41 has much longer coherence than all the others (about a factor of 6 longer than the longest T_2 of all the others), associated with a splitting of size 30 MHz. Other anomalies we discovered are related to the stability of a particular TLS in time. We find that the energy E_{ge} of some TLSs (about 5 %) changes spontaneously at varying time scales, from seconds to days. All the rest were remarkably stable [18].

Some of these changing TLSs have long lifetime (a few microseconds), which is consistent with the power-law trend we discussed above. Furthermore, we also measure a few representative TLSs as a function of temperature. We find no significant change in T_1 and T_2 below 100 mK, consistent with the expected [1] $\tanh(E_{\text{ge}}/2k_{\text{B}}T)$ dependence. We also find that the instability of some TLSs increases at elevated temperatures (i.e., the change in TLS energy becomes more frequent). We conclude that some of the TLSs we measure have a different nature, perhaps related to their internal structure or position inside the junction.

In conclusion, the energy decay and dephasing times of two-level defects in an AlO_x barrier of a Josephson junction are measured as a function of the coupling parameter with the phase qubit. The lifetimes vary substantially in our range of splittings, and agree with the theoretically predicted phonon radiative loss, which is dipole size dependent. The dephasing times show an ex-

tremum at intermediate couplings, which we attribute to an anti-correlated dependence on fluctuations in the environmental parameters which set the TLS energy. Such a dependence may distinguish between different theoretical models for TLSs. Our results demonstrate the power of the phase qubit as a dynamical coupling element to microscopic systems at the single microwave photon level.

We acknowledge fruitful discussions with Clare C. Yu. This work was supported by ISF grant 1835/07 and BSF grant 2008438.

-
- [1] W. A. Phillips, Reports on Progress in Physics, **Volume 50, Number 12**, 1657 (1987).
 - [2] A. Shnirman, G. Schon, I. Martin, and Y. Makhlin, Phys. Rev. Lett., **94**, 127002 (2005).
 - [3] L. C. Ku, and C. C. Yu, Phys. Rev. B, **72**, 024526 (2005).
 - [4] M. J. Kirton *et al.*, Semiconductor Science and Technology, **4**, 1116 (1989).
 - [5] N. Saks, Electron Device Letters, IEEE, **1**, 131 (1980), ISSN 0741-3106.
 - [6] J. M. Martinis *et al.*, Phys. Rev. Lett., **95**, 210503 (2005).
 - [7] G. Wendin and V. S. Shumeiko, ArXiv Condensed Matter e-prints (2005), arXiv:cond-mat/0508729.
 - [8] E. Tan, P. G. Mather, A. C. Perrella, J. C. Read, and R. A. Buhrman, Phys. Rev. B., **71**, 161401 (2005).
 - [9] K. B. Cooper *et al.*, Phys. Rev. Lett., **93**, 180401 (2004).
 - [10] E. Lucero *et al.*, Phys. Rev. Lett., **100**, 247001 (2008).
 - [11] R. W. Simmonds *et al.*, Phys. Rev. Lett., **93**, 077003 (2004).
 - [12] A. Lupascu, P. Bertet, E. F. C. Driessen, C. J. P. M. Harmans, and J. E. Mooij, Phys. Rev. B, **80**, 172506 (2009).
 - [13] P. Bushev *et al.*, ArXiv e-prints (2010), arXiv:1005.0773.
 - [14] M. Neeley *et al.*, Nat Phys, **4**, 523 (2008), ISSN 1745-2473.
 - [15] S. Oh *et al.*, Phys. Rev. B, **74**, 100502 (2006).
 - [16] G. Tettamanzi, *et al.*, in *2006 International Conference on Nanoscience and Nanotechnology* (2006).
 - [17] T. A. Palomaki, *et al.*, Phys. Rev. B, **81**, 144503 (2010).
 - [18] See supplementary material.
 - [19] J. P. Sethna, Phys. Rev. B, **25**, 5050 (1982).
 - [20] D. R. Lide, *CRC Handbook of Chemistry and Physics, 88th Edition* (CRC, 2007) ISBN 0849304881.
 - [21] J. M. Martinis, S. Nam, J. Aumentado, and C. Urbina, Phys. Rev. Lett., **89**, 117901 (2002).
 - [22] The qubit loop is coupled to an external bias source through a flux transformer, which sets the qubit energy [21].

Supplementary Material

EXPERIMENTAL DATA

The full data measured for 82 TLSs is presented in Table I and the $T_1(S)$, $T_2(S)$ and $T_\phi(S)$ values are plotted in figure 1. Figure 1a contains 82 data points while 1b contains only 42. For about 50% of the cases the dephasing time could not be determined, due to both low visibility and short dephasing time. This happens mostly for small splittings, which do not lie in the range of points presented in Fig. 3d of the main paper. For points that lie within this range and are omitted from the analysis we separately checked that the shorter coherence time does not affect the trend. The number of points in Fig. 1c is further reduced because for some T_1 limited TLSs we measured T_2 which is slightly longer than $2T_1$ due to measurement error. T_ϕ is excluded from the figure and table for these cases (three TLSs).

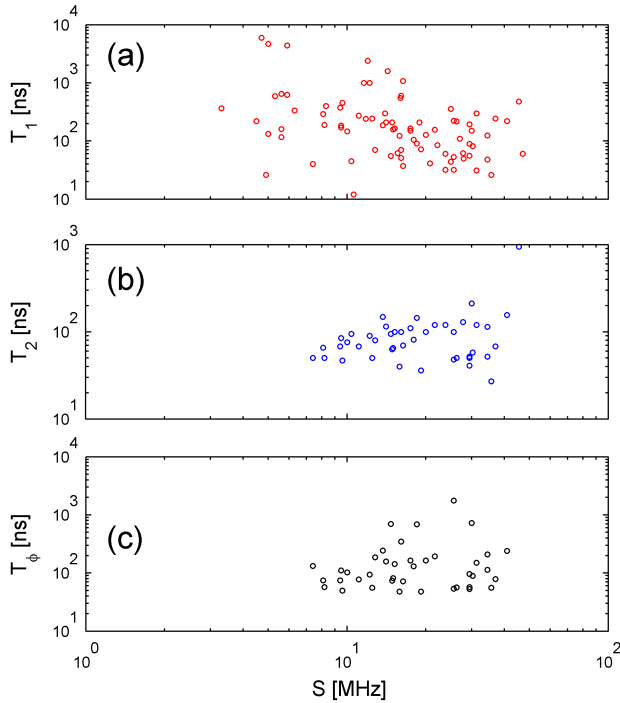


Figure 1: (a) Measured T_1 vs. splitting, (b) T_2 vs. splitting and (c) T_ϕ vs. splitting for all the measured TLSs. The spread in the T_1 data at a particular splitting value results from the random distribution of TLS orientation in the junction. It is apparent that the maximal lifetime shortens at larger splittings, consistent with dipole radiation. The spread of the T_2 data appears independent of the splitting, however the average values show some dependence which becomes more prominent in the dephasing times.

The errors in Fig. 3b and and Fig. 3c in the main

paper represent the statistical spread of the data within a 7 MHz window. They are calculated by normalizing the standard deviation by \sqrt{N} , where N is the number of points within the window.

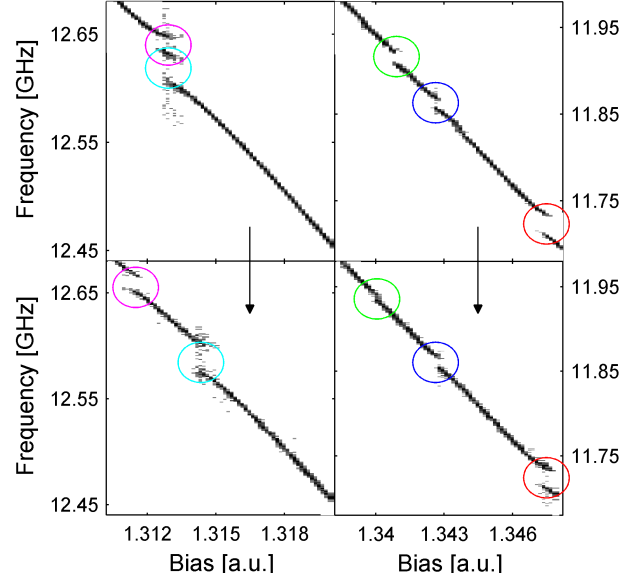


Figure 2: Qubit spectrum as a function of bias, before and after warmup to 1.5 K. Upper: two sections of the spectrum before warmup. Lower: the same sections, taken after heating the sample to 1.5 K and cooling down back to 10 mK. Circles with the same color indicate a splitting that we attribute to the same TLS. Both the position in frequency and splitting size of the TLSs are similar, indicating that the TLSs are not fully reset at this temperature.

We would like to point out that two points in Fig. 3c in the main paper have been excluded from the fit to a power law. These are the points with the largest average splittings (38 MHz and 46 MHz), where the statistics within each window is low (3 data points and 2 data points respectively). If we include these points in the fit we obtain an exponent $\alpha = -0.93$. We believe that the data points at the largest splittings may result from anomalous TLSs.

As pointed out in the main paper, some of the TLSs are changing in time. This is characterized by a change in the TLSs' transition energy, causing them to disappear from time to time (that is, to step out of our measurement bandwidth) or appear at a slightly different energy. An example of this phenomenon can be seen in Fig. 1 of the main paper. The leftmost TLS appears in the spectrum at larger bias value (that is smaller transition energy) than in the time-domain sweep. These two measurements were taken at an interval of one day.

New sets of TLSs are produced from the same device by

warming up to 20 K. We believe that some TLSs are not fully reset after warming up to only 1.5 K. Some splittings in the spectrum are similar in their frequency and splitting size to those before a partial warmup, as indicated in Fig. 2. Both the reset of TLSs at high temperatures, and the fact that some of the TLSs are changing in time indicate the true nature of the TLS as an approximation of a multilevel state, resulting from a multi-well energy structure.

STOCHASTIC SIMULATION

We reproduced the lifetime distribution of an ensemble of TLSs according to the TLS model in the following way. For each TLS we assume a uniform distribution of dipole orientation ($\cos \eta$ distributes uniformly, where η is angle relative to the electric field inside the junction), a potential asymmetry Δ from a uniform distribution

($\Delta \propto z$, where z is the effective distance between position states of the TLS inside the junction) and a tunneling energy Δ_0 from a log distribution ($\ln \Delta_0 \propto z$). These distributions are consistent with the TLS model, which assumes linear sensitivity of Δ on z and exponential sensitivity of Δ_0 on z . We excluded TLSs having smaller couplings than we can measure. For each TLS we compute the lifetime according to Eq. 1 in the main paper ($T_1(\sin(\theta)) = a/\sin(\theta)^2$, where $\theta = \arctan(\Delta_0/\Delta)$ and a is some constant). The simulation data points were then averaged over a 7 MHz window size, as done for the experimental data.

The resulting $\langle T_1(S) \rangle$ behavior (see Fig. 3c in the main paper, blue diamonds) resembles a sum of two power laws. At smaller splittings $S \lesssim S_{max}/2$, the points fit a power law with an exponent $\alpha_1 \approx -1.9$, while for larger splittings they fit a power law with an exponent $\alpha_2 \approx -1$. A similar trend is observed in our data as well.

f_{ge} [GHz]	S [MHz]	T_1 [ns]	T_2 [ns]	T_ϕ [ns]	CD No.
12.8	3.3	365	-	-	6
11.43	4.5	220	-	-	3
11.35	4.7	6000	-	-	7
12.45	4.9	26	-	-	7
11.55	5.0	4700	-	-	4
11.31	5.0	132	-	-	7
11.23	5.3	590	-	-	4
11.462	5.6	650	-	-	3
13.08	5.6	117	-	-	4
11.33	5.6	160	-	-	4
12.89	5.9	4400	-	-	6
11.4	5.9	623	-	-	6
12.79	6.3	335	-	-	4
13.11	7.4	40	50	133	4
12.85	8.1	291	66	74	3
12.13	8.2	190	50	58	5
11.57	8.3	400	-	-	4
11.45	9.4	373	68	75	5
11.835	9.5	170	-	-	2
11.342	9.5	185	85	110	2
12.26	9.6	453	47	50	2
12.32	10.0	147	76	102	5
11.85	10.4	45	95	-	4
11.6	10.6	12	-	-	6
12.25	11.1	275	68	78	7
12	11.6	1000	-	-	4
11.86	11.8	240	-	-	2
11.22	12.0	2400	-	-	1
11.88	12.2	1000	90	94	5
12.57	12.5	243	50	56	6
11.96	12.8	70	80	187	3
11.515	13.7	187	148	245	2
11.96	14.0	300	-	-	4
10.96	14.1	209	115	159	2
10.8	14.3	1600	-	-	7
13.22	14.7	55	95	697	6
11.57	14.9	210	63	74	3
11.27	15.0	158	65	82	5
12.24	15.2	165	100	143	3
11.7	15.6	62	-	-	4
11.38	15.9	123	40	48	7
11.59	16.0	550	-	-	7
11.78	16.1	51	-	-	5
11.62	16.1	70	100	350	5
10.95	16.1	600	-	-	1

f_{ge} [GHz]	S [MHz]	T_1 [ns]	T_2 [ns]	T_ϕ [ns]	CD No.
12.642	16.4	1080	70	72	2
11.85	16.4	37	-	-	7
12.41	17.5	165	110	165	5
12.37	17.5	150	-	-	7
12.542	18.0	106	81	131	8
11.42	18.5	91	144	690	4
11.915	18.9	208	-	-	2
12.47	19.2	72	36	48	6
11.21	20.0	127	100	165	5
12.73	20.8	41	-	-	7
11.86	21.7	156	120	195	2
12.15	22.2	85	-	-	7
11.72	23.8	60	120	-	2
12.66	23.8	32	-	-	7
12.44	25.0	44	-	-	6
11.86	25.0	355	-	-	1
11.61	25.6	53	100	1767	3
12.34	25.6	32	-	-	6
11.73	25.6	224	48	54	7
13.04	26.3	217	50	57	6
12.675	27.0	110	-	-	1
11.77	27.8	62	130	2687	4
12.2	28.0	50	-	-	1
12.613	29.4	56	52	97	2
11.22	29.4	89	41	53	2
12.67	29.4	193	50	57	3
12.147	30.0	150	212	723	8
12.34	30.3	82	58	90	4
11.89	31.3	31	-	-	6
10.91	31.3	300	120	150	7
12.78	34.5	125	114	210	5
12.12	34.5	48	52	113	6
11.59	35.7	26	27	56	2
11.17	37.0	243	68	79	6
11.772	41.0	220	156	242	1
12.05	45.5	476	950	-	4
11.99	47.0	60	-	-	1

Table I: Full measurement data of TLSs: TLS energy (f_{ge}), splitting (S), lifetime (T_1), coherence time (T_2) calculated dephasing time (T_ϕ) and cooldown number. The last column indicates which TLSs were measured on the same cooldown (i.e., temperature was not raised to more than 20 mK between measurements of TLSs belonging to the same cooldown).